Communications Earth & Environment https://doi.org/10.1038/s43247-026-03752-0

Article in Press

Compound atmospheric and soil droughts amplify the global loss of vegetation productivity

Received: 3 August 2025

Accepted: 3 June 2026

Cite this article as: Wang, Y., Miao, C., Huntingford, C. *et al.* Compound atmospheric and soil droughts amplify the global loss of vegetation productivity. *Commun Earth Environ* (2026). https://doi.org/10.1038/s43247-026-03752-0

Yufei Wang, Chiyuan Miao, Chris Huntingford, Yuanfang Chai, Jiachen Ji & Josep Peñuelas

Title: Compound atmospheric and soil droughts amplify the global loss of vegetation productivity

Authors: Yufei Wang [1], Chiyuan Miao [1*], Chris Huntingford [2], Yuanfang Chai [1], Jiachen Ji [1], Josep Peñuelas [3,4]

[1] State Key Laboratory of Earth Surface Processes and Disaster Risk Reduction, Faculty of Geographical Science, Beijing Normal University, Beijing 100875, China

[2] UK Centre for Ecology and Hydrology, Wallingford, Oxfordshire OX10 8BB, United Kingdom.

[3] CSIC, Global Ecology Unit CREAF-CSIC-UAB, Bellaterra, Catalonia 08193. Spain

[4] CREAF, Center for Ecological Research and Forestry Application, Cerdanyola del Vallès 08193, Catalonia, Spain

***Corresponding author**: Chiyuan Miao (miaocy@bnu.edu.cn).

Abstract:

Atmospheric droughts (high vapor-pressure deficit, VPD), soil droughts (low soil moisture, SM), and their compound occurrence (compound droughts, CDs) impose varying stress on terrestrial vegetation, yet their relative global impacts on productivity remain poorly quantified. Here, we assessed losses of gross primary productivity (GPP) during growing seasons from 1982 to 2018 under high VPD alone, low SM alone, and CDs. CDs caused the greatest GPP reductions (−8.94 g C m^{-2} per event), nearly four times the losses from high VPD (−2.24 g C m^{-2}) or low SM (−2.20 g C m^{-2}) events. Broadleaf forests were most affected by CDs and high VPD, while needleleaf forests were more sensitive to low SM. Meteorological factors, particularly temperature and precipitation, were key drivers of the three types of droughts contributing to GPP losses. GPP reductions from high VPD were broadly associated with temperature, while drivers under low SM varied spatially. Vegetation recovery after CDs was slower than after high VPD or low SM events in over 60% of regions, and it was more difficult to fully achieve. Our findings clarify how atmospheric and soil droughts jointly limit productivity, providing insight for improved assessments of vegetation carbon uptake under changing climate conditions.

Introduction

Terrestrial ecosystems are crucial global carbon sinks, partially offsetting current carbon dioxide (CO_2) emissions to the atmosphere caused by human burning of fossil fuels [1]. Vegetation, a key component of land ecosystems, interacts closely with soil and the atmosphere, notably affecting the carbon balance and the water cycle, and it can feed back on climatic conditions [2–5]. Plants absorb CO_2 during photosynthesis and convert it into organic matter [6], a process quantified as gross primary productivity (GPP). Drought, a major type of natural disaster, strongly affects GPP at regional and global levels. Water stress during drought inhibits vegetation growth by altering plant structure and physiology, slowing photosynthesis and reducing GPP [7]. Climate change has increased the frequency and intensity of droughts worldwide [8–11], adversely affecting terrestrial GPP through changes in hydrological and climatic conditions [12]. Observational evidence indicates that global vapor-pressure deficit (VPD) has increased and soil moisture (SM) has declined over recent decades [13,14]. The need to understand the impact of drought on GPP is therefore urgent, because this knowledge is essential for formulating relevant policies to reduce the risk of drought and maintain the stability of the carbon cycle in terrestrial ecosystems [15].

Atmospheric and soil droughts are the primary stressors that limit water use and carbon uptake in terrestrial ecosystems [14,16,17]. Atmospheric drought, characterized by a high VPD, not only exacerbates water deficits on the terrestrial surface from evaporation and vegetation transpiration, but more importantly also triggers plants to close their stomata to reduce CO_2 uptake, thereby limiting photosynthesis [14,18,19]. Soil drought, characterized by a low level of SM, directly limits plant photosynthesis by restricting water uptake by roots [20,21]. The interaction between high VPD and low SM frequently leads to a compound drought (CD), where the two conditions coexist [22]. Low SM and high VPD often coincide globally, because insufficient SM decreases evapotranspiration and increases sensible heat flux, leading to a warmer, drier atmosphere with elevated VPD, which in turn increases evaporative water losses, further reducing SM [20,23,24]. These two types of positive feedback loop between SM and VPD may pose a strong threat to vegetation growth, the effects of which require evaluation. Such feedbacks are likely to strengthen further under global warming, which also requires quantification. However, a key initial starting point is to use available data in a manner that enhances understanding of the contemporary

climatic state.

Many previous studies have analyzed the impact of a single type of drought on vegetation, focusing primarily on either atmospheric (e.g., high VPD) or soil (e.g., low SM) conditions [25–29]. Meteorological factors above ground and SM below ground, however, influence vegetation growth in different ways and to varying degrees [30]. It is therefore essential to clearly distinguish the processes and mechanisms through which they affect vegetation. The relative roles of VPD and SM in the carbon–water cycle in affecting vegetation are attracting increasing attention, and some initial studies have begun to investigate impacts of compound forcing during extreme events [31]. Recent studies have found that global vegetation has become more sensitive to SM variability over the last three decades, as climatic conditions change [32]. The dominant role of SM in determining drought stress on vegetation, however, is not universal [21]. The efficiency of ecosystem production in humid biomes is constrained more by high VPD than by low SM [17]. This finding highlights the spatial heterogeneity of ecosystem productivity in response to soil moisture conditions and atmospheric water vapor demand conditions. Another challenge is that the coupling between vegetation and compound droughts has intensified, particularly in regions with limited water or energy resources [33,34]. Therefore, the impacts of compound SM and VPD droughts on vegetation are more complex and cause larger losses than the impacts of single-cause droughts (i.e., droughts associated with either low SM or high VPD alone) [22–24]. This finding is particularly concerning because the intensity and frequency of such CDs, and the associated GPP losses, have been increasing in recent decades [33,35]. Furthermore, meteorological factors such as radiation, temperature, and precipitation are key drivers of vegetation–CD coupling, each exerting complex direct and indirect effects [34]. CDs, however, typically occur under extreme climatic conditions, raising the question of whether they are indeed more destructive to vegetation than are the more commonly occurring single-cause droughts. The responses of vegetation to drought also vary with local climate and vegetation type. Previous studies have examined single drought types, but a comprehensive assessment of the comparative impacts of compound vs. single droughts on GPP at a global scale is lacking. Accurately quantifying GPP losses from compound, atmospheric, and soil droughts—and comparing their relative impacts at the global scale—is therefore essential for understanding the vulnerability of ecosystems in a changing climate.

We compared GPP during 1982–2018 under atmospheric droughts alone (here termed "high VPD"), soil droughts alone (here termed "low SM"), and CDs with GPP under normal climatic conditions; we quantified vegetation losses in global terrestrial ecosystems due to these three types of droughts during vegetation growing seasons (April–September in the Northern Hemisphere and October–March in the Southern Hemisphere). We used geographic detectors and partial correlation analyses to determine how climate, the characteristics of drought, and soil nutrients contributed to GPP losses during droughts. Finally, we also quantified the time needed by vegetation to recover following compound and single-cause droughts. Our study posed three questions: (1) What are the global spatial distributions of vegetation losses from CDs and from high VPD and low SM? (2) What are the primary drivers of vegetation damage following these droughts? (3) How much time is needed for GPP to recover to normal after these droughts?

Results

Characteristics of droughts

Overall, low SM tended to last longer than both CDs and high VPD, persisting for about 2–3 months per year compared with 1–1.2 months per year for CDs and high VPD (Fig. 1a–c, 1j). Single-cause droughts were more frequent than CDs but were generally less intense. Droughts with high VPD and low SM occurred at an average frequency of above 0.8 times per year, whereas CDs occurred 0.2–0.4 times per year, equivalent to once every 2–3 years (Fig. 1d–f, 1k). CD intensity typically exceeded 0.8 in most regions, and high-VPD intensity averaged around or below 0.8. Low-SM intensity was generally <0.5, with only limited regions such as the Amazon Basin and central Africa having slightly higher intensities (Fig. 1g–i).

The duration and frequency of CDs, high VPD, and low SM all tended to increase (Fig. 1j, k). Specifically, the frequency of high VPD increased markedly, by an average of 0.013 events per year. In comparison, the frequencies of CDs and low SM increased by an average of 0.0035 and 0.0037 events per year, respectively (Fig. 1k). The intensities of the three types of droughts were generally unstable and fluctuated over the study period (Fig. 1l).

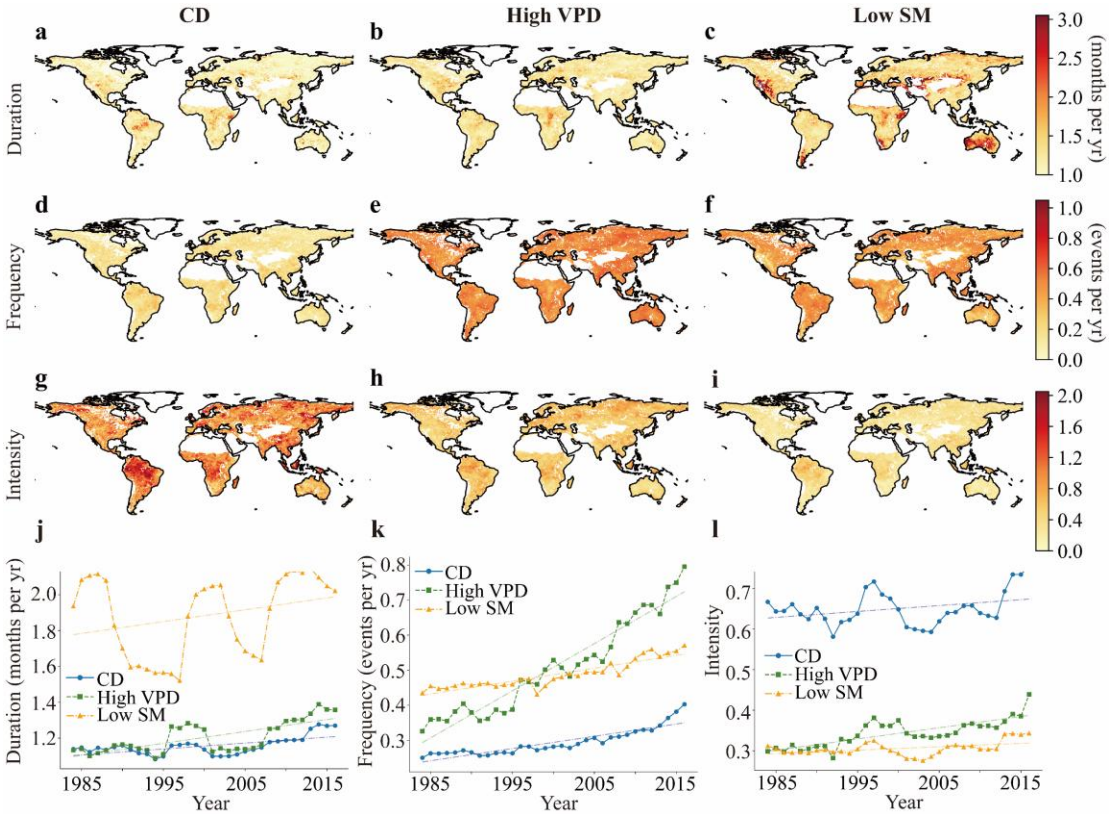

Fig. 1 Spatial and temporal patterns of drought characteristics during the growing season for 1982–2018. a–i Average duration, annual count, and average intensity. **j–l** Temporal trends of these characteristics for the three drought types during the study period, analyzed using an average 5-year sliding window. The x-axis marks the starting year of each window.

GPP losses under the influence of droughts

GPP losses (indicated using negative values) were typically larger for CDs than for single-cause droughts. Average GPP losses under CDs were −8.94 g C m^{-2} per event (median: −5.16) compared with −2.24 and −2.20 g C m^{-2} per event for high VPD and low SM, respectively (medians: −1.69 and −1.70, respectively) (Fig. 2a–c). GPP losses under CDs exceeded −50 g C m^{-2} per event in nearly 30% of the study area, whereas <3% of the area had such extreme losses under single-cause droughts. The strongest CD-induced decreases in GPP were in the mid- and high-latitudinal regions of the Northern Hemisphere (eastern North America, Eurasia around 60°N, and eastern China) and in the mid- to low-latitudinal regions of the Southern Hemisphere (eastern South America, central Africa, and eastern Australia). High VPD also led to gains in GPP in colder high-latitudinal regions, with a spatial pattern similar to that of the CDs, and the

beneficial effects of low SM were smaller in these regions. We also analyzed the seasonal variation in GPP losses (Fig. S1). The results indicate that GPP reductions under all three drought types were typically during summer and early autumn.

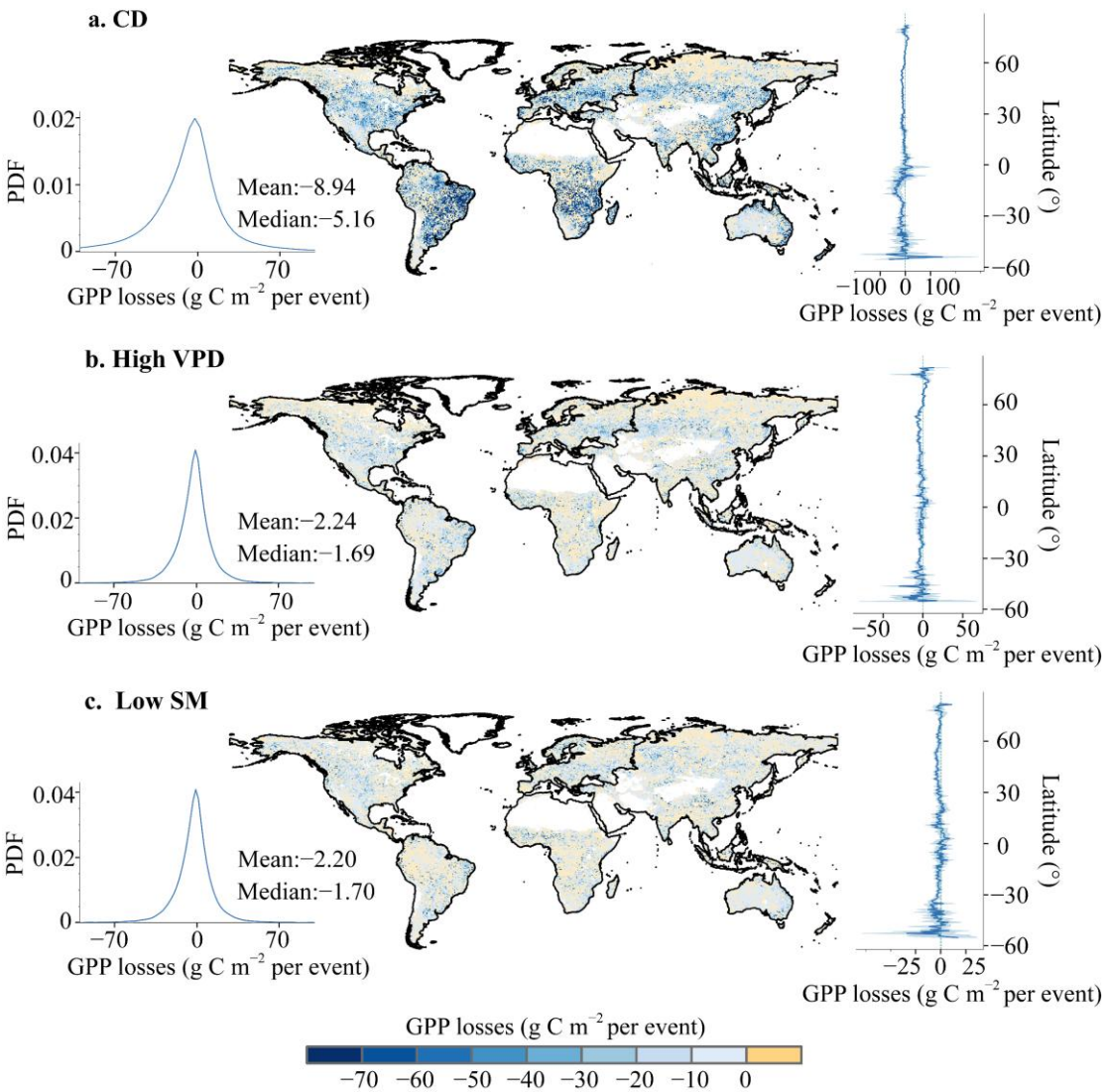

Fig. 2 Average GPP losses under the influence of compound and single-cause droughts during the growing season from 1982 to 2018. a, b, c Average GPP losses under the influence of CDs, high VPD, and low SM, respectively. Negative values indicate amounts of GPP lost under the influence of droughts, and positive values indicate amounts of GPP gained under the influence of droughts compared with normal climatic conditions; the more negative the value, the larger the losses of vegetation GPP.

GPP losses under CD conditions were largest for broadleaf forests (Fig. 3a), followed by rainfed crops. The pattern was similar during high VPD. Under conditions of low SM, however, needleleaf forests lost more GPP than did other types of vegetation. Except in hyper-arid regions, GPP losses were greater under

CDs than under the other drought types across all climate zones. Within humid regions, GPP losses under all three drought types were relatively small at higher latitudes, but more pronounced in the monsoon regions of eastern China and eastern South America. The most severe GPP losses under all three drought types occurred mainly in dry subhumid and subhumid regions at low and mid latitudes of the Southern Hemisphere (Fig. 3b).

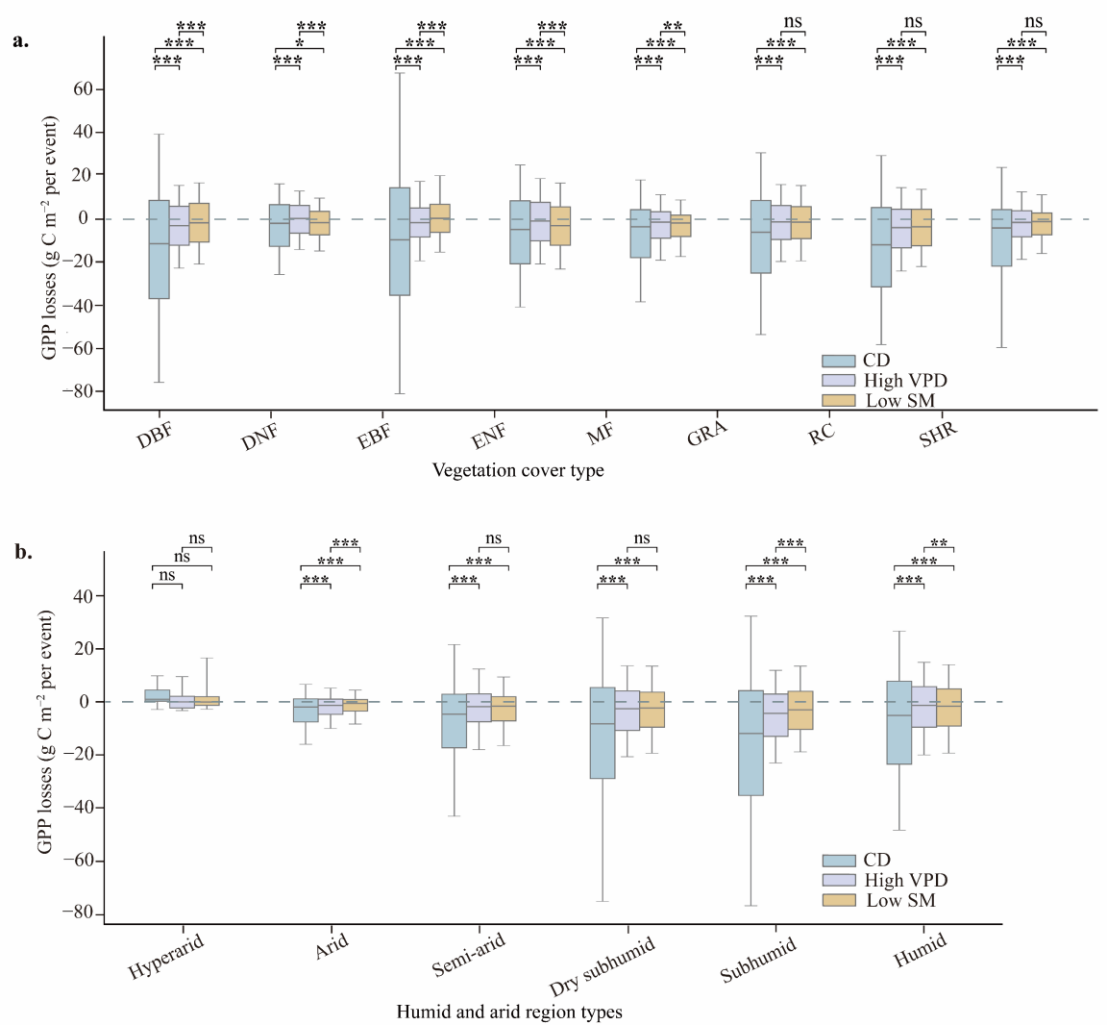

Fig. 3 GPP losses across vegetation types and climatic zones. a and **b** GPP losses across vegetation cover types and climatic zones, respectively. The boxes indicate the interquartile range (25th to 75th percentiles), the horizontal lines in the boxes indicate the median values, and the whiskers extend to the 10th and 90th percentiles. The two gray horizontal dashed lines indicate a loss of 0. DBF, deciduous broadleaf forest; DNF, deciduous needleleaf forest; EBF, evergreen broadleaf forest; ENF, evergreen needleleaf forest; MF, mixed forest; GRA, grassland; RC, rainfed crop; SHR, shrubland. ***, **, *, ns represent $p<0.001$, $p<0.01$, $p<0.05$, and $p>0.05$, respectively, according to the two-sided Mann–Whitney U test.

Analysis of factors affecting GPP losses caused by drought

The results for the "geographic detectors" method indicate that meteorological factors, particularly temperature and precipitation, were key drivers of the three types of droughts contributing to GPP losses, and their spatial distribution is quite complex (Figs. 4, S2). GPP losses under high VPD had broader spatial correlations with temperature than did CDs and low SM (Figs. 4b, S2b). While temperature exerted negative impacts on GPP caused by high VPD in 24%–33% of regions, it showed positive effects in certain high-latitude and high-altitude areas, thereby enhancing GPP locally. Temperature was the dominant factor in the losses caused by low SM (Figs. 4c, S2c). In addition, drought intensity also proved to be a crucial factor. Factors affecting GPP losses caused by low SM were highly spatially heterogeneous, with drought intensity playing a larger role across southern and southeastern Asia, affecting 28%–37% of the study area.

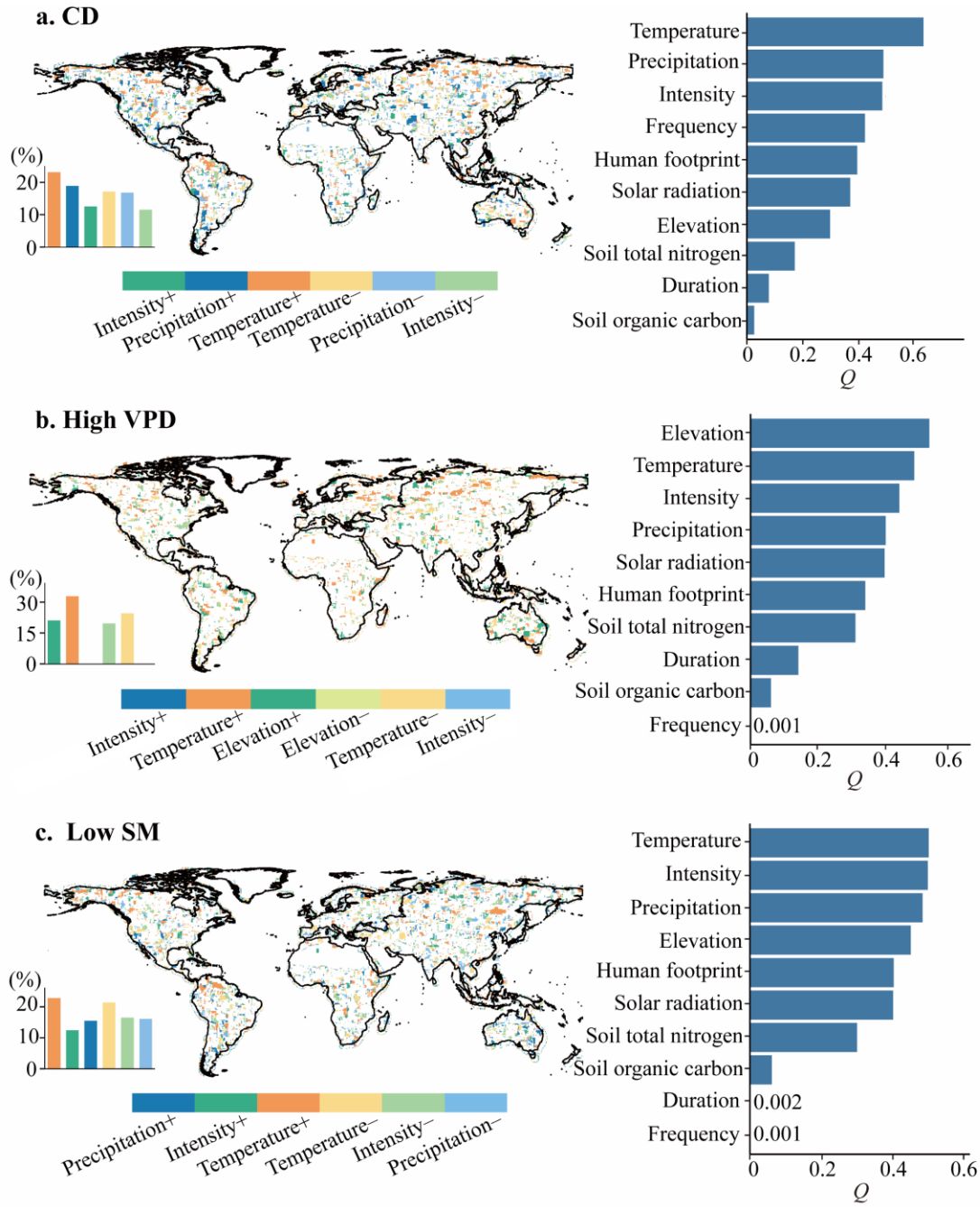

Fig. 4 Relative contributions of factors influencing GPP losses. The blue bars in **a–c** represent the relative contributions of several factors influencing the GPP losses caused by CDs, high VPD, and low SM, respectively (see Text S1 for the derivation of *Q*). The spatial distributions indicate the attribution of the locally most dominant factors associated with GPP losses. The dominant factor is identified as the factor with the largest absolute partial correlation coefficient: "+" and "–" denote positive and negative correlations, respectively. The small bar graphs accompanying each map show the percentage of total land area where each factor has the most influence on GPP losses.

Post-drought GPP recovery time

Vegetation recovery time following CDs was predominantly within 2–5 months. Extended recovery periods (≥6 months) were primarily in mid- to high-latitudinal regions of the Northern Hemisphere, corresponding to areas with severe GPP losses (Fig. 5a). In contrast, recovery time following single-cause droughts was more variable across regions (Figs. 5b, S3a, b). We quantified the difference in recovery time between CDs (Fig. 5a) and single-cause droughts (Fig. S3a, b) as ΔRT, representing the relative extension or shortening of recovery time following CDs compared with following high VPD or low SM (Fig. 5c, d). Recovery time was longer following CDs than it was following single-cause droughts in >60% of the study area, and half of the regions experienced a 1- to 2-month delay. Regions in which recovery time was shorter following CDs than it was following high VPD were mainly in the high latitudes of the Northern Hemisphere and mid-latitudes of the Southern Hemisphere (e.g., the South African Plateau and most parts of Australia). In comparison, regions in which recovery time was shorter following CDs than it was following low SM were mainly at higher latitudes of the Northern Hemisphere and in central to eastern Australia. As a broad generalization of our findings, the differences between the recovery times of CDs and those of high VPD and low SM events are relatively small compared with the differences observed in other quantities such as intensity and impact on GPP suppression. Additionally, we found that the percentage of pixels where GPP failed to recover was higher following CDs than following high VPD or low SM, regardless of whether the recovery time exceeded one or two years (Fig. S4). This suggests that CDs are more likely to cause permanent damage to vegetation.

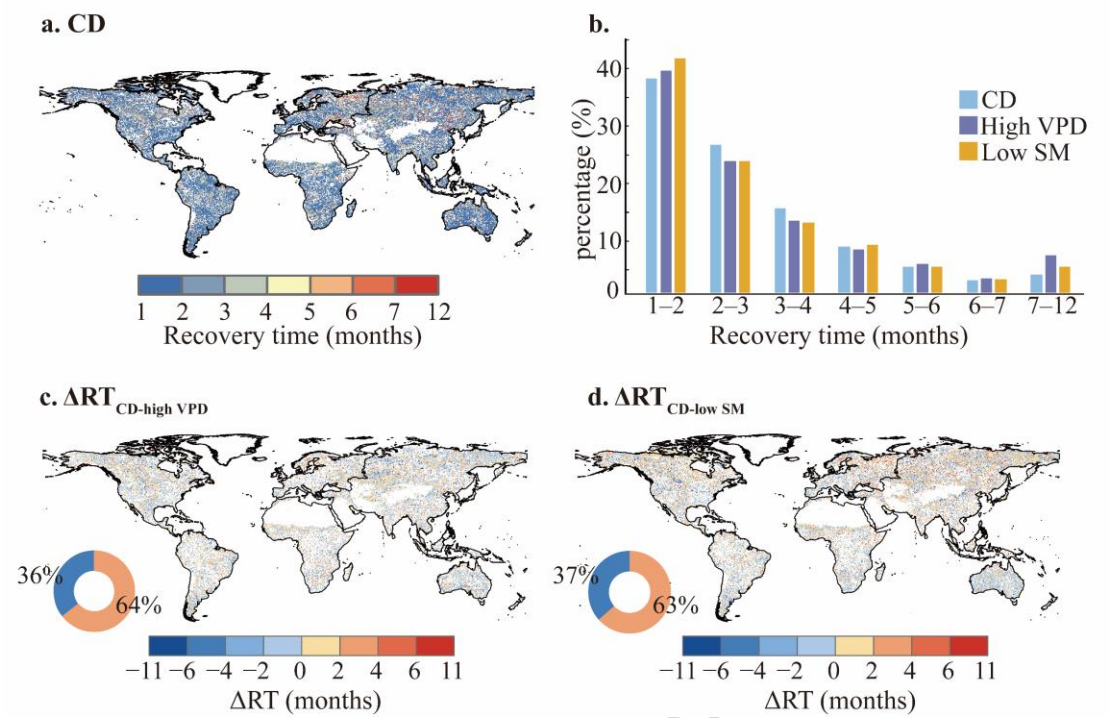

Fig. 5 Recovery time and differences in recovery time (ΔRT) during the growing seasons from 1982 to 2018. a Recovery time following CDs. **b** Percentages of the study area corresponding to different recovery times. **c** Geographic differences in recovery time between CDs and high VPD. The orange and blue segments in the accompanying inset circular charts represent the proportions of grid cells with ΔRT greater than and less than zero, respectively. **d** is the same as **c**, but for CDs and low SM.

Across vegetation types (Fig. 6a), deciduous broadleaf forests, evergreen needleleaf forests, and grasslands all exhibited longer recovery time following CDs than after single-cause droughts. Looking at wet versus dry regions (Fig. 6b), recovery time following CDs in wet regions, especially humid regions, was longer than it was in dry regions, with a more significant difference compared with recovery time for single-cause drought events.

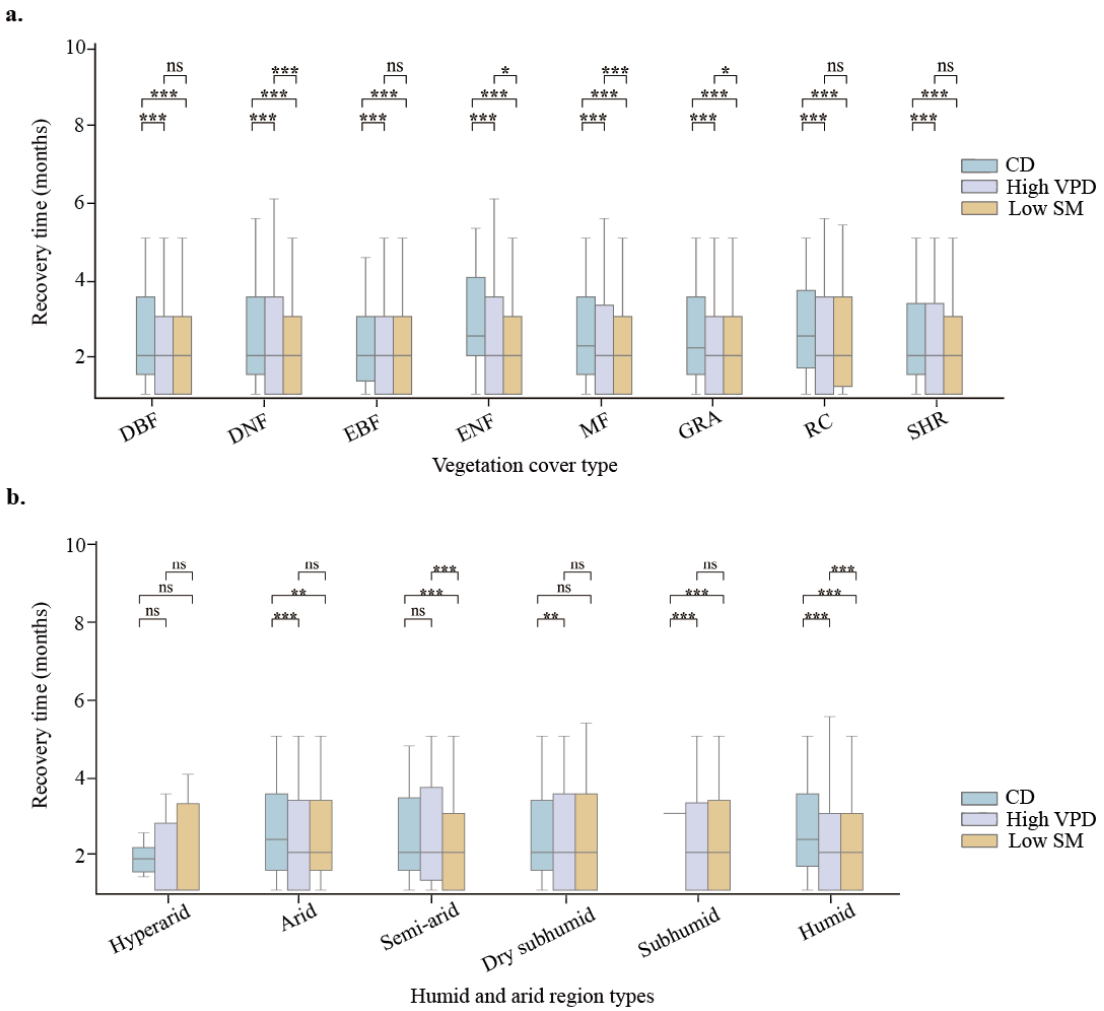

Fig. 6 Recovery times across vegetation types and climatic zones. a and **b** Recovery times across vegetation cover types and climatic zones, respectively. The boxes indicate the interquartile range (25th to 75th percentiles), the horizontal lines in the boxes indicate the median values, and the whiskers extend to the 5th and 95th percentiles. DBF, deciduous broadleaf forest; DNF, deciduous needleleaf forest; EBF, evergreen broadleaf forest; ENF, evergreen needleleaf forest; MF, mixed forest; GRA, grassland; RC, rainfed crop; SHR, shrubland. ***, **, *, ns represent $p<0.001$, $p<0.01$, $p<0.05$, and $p>0.05$, respectively, according to the two-sided Mann–Whitney U test.

Discussion

Differential responses of vegetation to drought: physiological and environmental drivers

Our results indicate that CDs caused larger vegetation losses than did single-cause droughts, a pattern associated with their distinct characteristics. Studies have demonstrated that vegetation acclimated to long-term mild droughts is more resistant than vegetation experiencing short-term severe droughts [36–38]. Vegetation may therefore respond to drought more quickly and suffer larger losses in a short period of time under low-frequency but high-intensity CDs. GPP also had more severe losses under the influence

of CDs than under the influence of high VPD and low SM in the mid- and low-latitudinal regions of the Southern Hemisphere (excluding the Amazon Basin) compared with other regions. Research has demonstrated that vegetation growth in tropical regions is highly responsive to variations in precipitation and temperature during the dry season [29]. Decreased precipitation and increased temperature in the dry season will decrease vegetation's access to water and increase its vulnerability to drought. Increased precipitation during the rainy season enhances the effective soil moisture available to plants, facilitating vegetation growth [39]. Thus, most species of tropical vegetation grow rapidly in the rainy season by using sufficient water to store nutrients, and grow slowly in the dry season to reduce energy consumption [40]. Although temperature and VPD are often lower during the rainy season, favoring vegetation transpiration, reduced light availability and increased cloud cover are often the primary constraints on net CO_2 uptake by vegetation[40]._ Vegetation growth under conditions of high VPD is initially suppressed by increased transpiration and high temperatures, but plants can partially compensate by absorbing more soil moisture. Similarly, VPD and solar radiation under conditions of low SM can still decisively regulate transpiration to adapt to deficits of soil moisture [39,40]. In contrast, the interaction between low SM and high VPD under CDs amplifies the negative impact on vegetation and destroys its ability to regulate water and, thus, its survival strategy.

Vegetation losses in the mid-latitudes of the Northern Hemisphere were high under the influence of the three types of droughts, consistent with previous research results [33,41]. Water constraints strongly affected vegetation growth in the mid-latitudes of the Northern Hemisphere. By contrast, increases in GPP are chiefly concentrated in high-latitude boreal regions, where vegetation is typically limited by energy rather than water availability. When high VPD or low SM occurs, the temperature and radiation usually increase [41]. The positive effects of these phenomena can often outweigh the negative effect of drought, resulting in a net increase in GPP. In addition, in most parts of the Amazon, GPP also increased under low SM conditions. This is related to the seasonality of rainfall and the fact that the region is humid. Many trees with deep root systems can obtain deeper soil moisture, so an increase in GPP can be observed in the short term [29].

Vegetation in arid regions exhibits high water use efficiency and drought resistance due to long-term adaptation mechanisms. Furthermore, the inherently low GPP in arid regions limits the absolute magnitude of potential losses under the influence of drought[7] In humid regions, drought impacts on vegetation are strongly shaped by hydroclimatic background and plant water-use strategies[42]. In the monsoon regions of eastern China and eastern South America, ecosystems depend strongly on current rainfall because vigorous growth and high transpiration coincide with highly seasonal precipitation and rapid soil-moisture turnover, making vegetation carbon uptake particularly vulnerable to drought[42]. In the low- to mid-latitude transition zones between humid and dry regions of the Southern Hemisphere, high interannual precipitation variability and the dominance of shallow-rooted grasses and shrubs further increase sensitivity of vegetation to drought. We also found that broadleaf forests lost more productivity than other vegetation types under conditions of both CD and high VPD. This heightened vulnerability is due to their physiological structure, with large leaf areas and thin cuticles that promote high rates of transpiration and substantial capacities to store water, allowing them to respond quickly to changes in the atmospheric environment [43]. Needleleaf trees, with their small leaves and narrow tracheids, have lower capacities to transport water than do broadleaf trees. Their thick, waxy cuticles, however, reduce the rate of transpiration, allowing them to maintain high photosynthetic capacities during short-term atmospheric droughts [44]. Coniferous trees have deep roots and can use soil moisture with relatively high efficiency. We found, however, that coniferous forests still had relatively large GPP losses when SM was low (Fig. 3a). This loss may have been caused by the characteristics of soil drought or other non-climatic factors (Fig. 4c). For example, Bauke et al. (2022) [45] suggested that soil drought restricts nutrient mobility in soil water, decreasing nutrient uptake by trees and affecting their growth and productivity.

Mechanisms of recovery time after the three types of droughts

Vegetation recovered faster (1–2 months) from single-cause droughts than from CDs (Fig. 5b). This pattern of differential recovery indicated the lower severity of high VPD or low SM as individual stressors relative to CDs (Fig. 1g–i), leading to less physiological damage and consequently the capacity to recover more quickly [46]. Interestingly, the proportion of areas where recovery time was >7 months was slightly higher after high VPD and low SM (Fig. 5b) than after CDs. This anomaly may represent the longer

duration and more frequent occurrence of high VPD and low SM.

Recovery in arid and semi-arid areas is often more restricted by SM and climatic conditions compared with recovery in humid areas. Dryland plants possess drought-resistance genes as an adaptation to long-term water scarcity, but persistent extreme droughts pose unique challenges. High rates of evaporation of soil water coupled with slow recharge capacity slow the rate of growth of arid-adapted species. These combined factors ultimately prolong the periods of recovery in arid ecosystems [47]. Vegetation in humid areas can usually support faster recovery by faster water cycles and water surpluses in non-drought periods [48]. The time needed for vegetation to recover in different regions, however, depends on the climatic conditions in which a local drought occurred [49,50] and on the variability of the thresholds of recovery time.

Implications and limitations

Our findings highlight that compound drought events pose a notably greater threat to terrestrial ecosystems than single-cause droughts, especially considering their higher severity, extended recovery times, and spatial variability. This underscores the importance of incorporating the combined effects of atmospheric and soil droughts into drought risk assessments, climate modeling, and ecological management practices, particularly in regions where vegetation recovery is prolonged. However, it should be noted that this study still has some limitations. In this study, the thresholds for high VPD and low SM were empirically set at the 90th and 10th percentiles, respectively. However, this approach does not account for the fact that drought sensitivity may vary across ecosystems and regions, potentially resulting in region-specific threshold differences. Additionally, the vegetation type from 2018 was used to represent the entire study period (1982–2018), without accounting for potential changes in land use that could influence GPP and drought responses. We removed the seasonal cycle of GPP to minimize the impact of agricultural management practices (such as sowing, irrigation, and harvesting) on vegetation at specific times of the year [51,52] (See the Methods section). Furthermore, the growing season used in this study was defined as a fixed time window, which is appropriate for analyses at the monthly scale[53]. However, at finer temporal scales and over smaller spatial extents, vegetation activity and phenology are likely to exhibit substantial spatial heterogeneity, because the climatic and hydrological controls on vegetation

growth, including temperature, radiation and precipitation, vary across region[54,55]. For example, the April–September growing season adopted here for the Northern Hemisphere is generally suitable for temperate ecosystems, but in reality the growing season is shorter in cold high-latitude regions, occurs earlier in Mediterranean ecosystems[56,57], and indistinct in some equatorial tropical rainforests[58]. Future work should therefore incorporate vegetation phenology by adopting dynamic growing-season definitions for a more precise assessment of drought impact. Another consideration is that this study examined the vegetation recovery time following drought, but in some regions, vegetation does not return to pre-drought levels even several years after the drought has ended. Therefore, it is necessary to explore the degree of vegetation recovery in these areas within a specific period of time and the reasons behind it, investigating long-term ecosystem feedbacks to increasingly frequent and severe CDs, including impacts on global carbon budgets.

Data and Methods

Data

Monthly GPP data sets from 1982 to 2018 were derived from Wang et al. (2020) [59] with a spatial resolution of 0.05°. The data were based on about 40 years of remotely sensed Advanced Very High Resolution Radiometer (AVHRR) data and hundreds of flux-site observations around the world and were obtained using evaluations of near-infrared reflectance (NIRv). Analysis at the level of 104 flux sites around the world indicated that NIRv could accurately identify GPP ($R^2 > 0.71$), but it may not perform as well as other methods in certain vegetation types (e.g., C4 plants), which is an uncertainty of this method. Machine-learning upscaling methods, models of light-use efficiency (LUE) models, and process-based models have indicated that these data are highly consistent with flux sites and models and superior to other GPP products, which is helpful for estimating global terrestrial carbon flux [60–62].

The simultaneous monthly reanalysis data for surface 2-m temperature, precipitation, 2-m dew-point temperature, soil moisture, and near-surface solar radiation from 1982 to 2018 were all obtained from the ECMWF Reanalysis v5 (European Centre for Medium-Range Weather Forecasts, ERA5), monthly averaged data on single levels with a spatial resolution of 0.25° × 0.25° [63]. To enhance the robustness of

the affecting-factors analysis results, we also used ground-based observed monthly data for surface 2-m temperature and precipitation from the Climatic Research Unit Time Series 4.09 (CRU). Land-cover data were obtained from the European Space Agency Climate Change Initiative (ESA CCI), which provides a high-quality, consistent, and long-term time series from 1992 to 2022. We divided the terrestrial surface into different types of vegetation for further analysis, using 2018 data at a resolution of approximately 300 m. We classified eight vegetation types (Fig. S5), and for farmland, we excluded irrigated agricultural areas, focusing only on rainfed agricultural regions to minimize the influence of human activities. We unified all data to a monthly scale and a spatial resolution of 0.5° × 0.5° by using nearest neighbor interpolation.

Methods

Drought metric selections

Traditional meteorological drought indices primarily represent precipitation deficits (such as the Standardized Precipitation Index, SPI) or the balance between precipitation and evapotranspiration (such as the Standardized Precipitation Evapotranspiration Index, SPEI; and the Palmer Drought Severity Index, PDSI) [64]. The SPI is based solely on precipitation, while the SPEI and PDSI incorporate the effect of temperature by accounting for potential evapotranspiration (PET). Moreover, the PDSI incorporates soil available water capacity information [12], which is less suitable for isolating purely meteorological drought than are atmospheric indicators such as VPD. VPD, on the other hand, indicates the potential for water extraction from the soil and plant surface (stomata). Under high VPD conditions, plants close their stomata to reduce water loss through transpiration, limiting CO_2 absorption and thus inhibiting photosynthesis. Chronic high VPD can also lead to xylem embolism, triggering hydraulic failure and increasing the risk of tree mortality, further impacting plant phenology and carbon allocation strategies. These physiological processes cannot be directly quantified by drought indices like the SPI, SPEI, and PDSI [14,65,66]. In addition, we used soil moisture as the soil drought indicator because it can most simply and intuitively represent the soil drought situation [32].

Calculation of VPD

We used gridded monthly data for 2-m temperature and 2-m dew-point temperature to calculate VPD (kPa):

$$SVP=0.611\times \exp\left(\frac{17.27\times T_a}{T_a+237.3}\right) \quad (1)$$

$$AVP=0.611\times \exp\left(\frac{17.27\times T_d}{T_d+237.3}\right) \quad (2)$$

$$VPD=SVP-AVP \quad (3)$$

where T_a is the monthly average surface air temperature (℃), T_d is the monthly average dew-point temperature (℃), SVP is the saturation vapor pressure (kPa), and AVP is the actual vapor pressure (kPa).

Definitions of compound and single-cause droughts

High VPD and low SM may each extend over multiple months [10,67], so we standardized the temporal unit to a monthly scale to ensure consistency in comparing drought types. Droughts were identified using percentile-based thresholds (Fig. 7). High VPD was defined as monthly VPD exceeding the 90th percentile for the corresponding month over the study period. Similarly, low SM was defined as monthly SM below the 10th percentile [22]. A CD was defined as one or more consecutive months during which both high VPD and low SM occurred; i.e., a single month meeting these conditions was counted as one CD, and a continuous sequence of such months was also treated as one CD. Similarly, any months meeting only one of the two conditions were identified as months with single-cause droughts, and one or more consecutive occurrences of these months were grouped into either high VPD or low SM, depending on the condition met. In addition, in the treatment of drought events that begin at the end of one year and continue into the next year, we considered four situations. See Text S3 in the Supplementary Information for details.

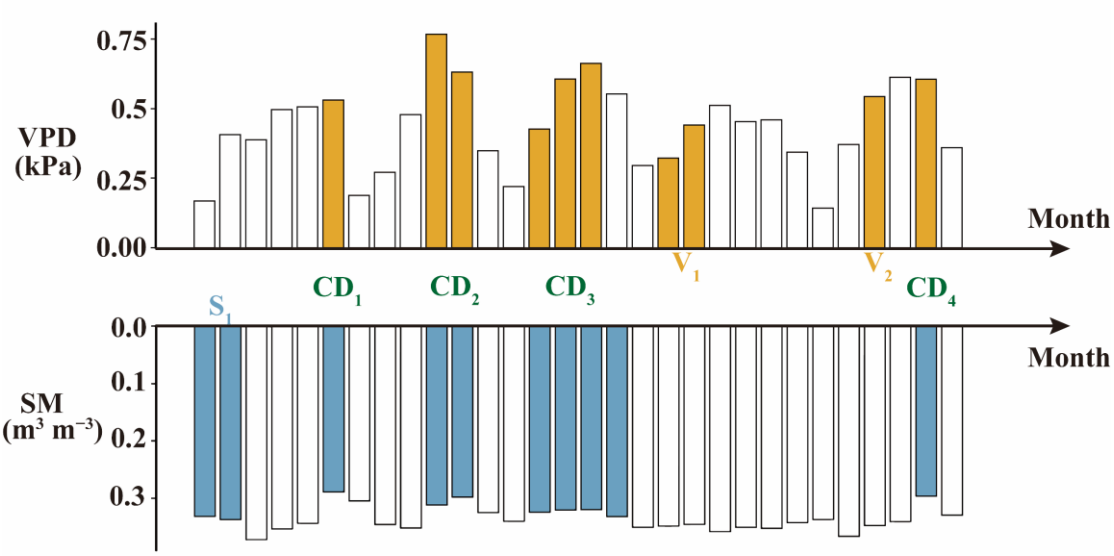

Fig. 7 Schematic diagram of droughts. Monthly VPD and SM are shown as bar charts. Orange bars indicate VPD exceeding the 90th percentile for the corresponding month during the study period; blue bars indicate SM below the 10th percentile for the corresponding months. V_1 and V_2 represent high VPD, and S_1 represents low SM. CD_1, CD_2, CD_3, and CD_4 represent four CDs.

Drought characteristics were described by duration, frequency, and intensity during the growing season from 1982 to 2018. Duration was defined as the total number of months a drought persisted, and frequency was quantified as the number of droughts occurring during the study period (average per year). Intensity refers to the severity of the drought. For CDs, it means the degree to which VPD exceeded the baseline (the 90th percentile VPD) while SM was lower than the baseline (10th percentile SM) at the same time. For high VPD, it means the degree to which VPD exceeded the baseline (90th percentile VPD) when SM was at a normal level. For low SM, it means the degree to which SM was lower than the baseline (10th percentile SM) when VPD was at a normal level [33]:

$$Intensity(CD)=\sqrt{\frac{\Sigma\left(\frac{VPD_i-VPD_{90th}}{VPD_\sigma}\right)^2+\Sigma\left(\frac{SM_i-SM_{10th}}{SM_\sigma}\right)^2}{2D}} \quad (4)$$

$$Intensity(high\ VPD)=\sqrt{\frac{\Sigma\left(\frac{VPD_i-VPD_{90th}}{VPD_\sigma}\right)^2}{D}} \quad (5)$$

$$Intensity(low\ SM)=\sqrt{\frac{\Sigma\left(\frac{SM_i-SM_{10th}}{SM_\sigma}\right)^2}{D}} \quad (6)$$

where $Intensity(CD)$, $Intensity(high\ VPD)$, and $Intensity(low\ SM)$ are the intensity of a CD, a high VPD, and a low SM, respectively; VPD_i is the value of VPD in month i, VPD_{90th} is the 90th percentile

VPD for that month, VPD_{σ} is the standard deviation of VPD for the month, SM_i is the level of SM in month i, SM_{10th} is the 10th percentile SM for that month, SM_{σ} is the standard deviation of SM for the month, and D is the duration of the drought, defined as the number of consecutive dry months. The summations (and related summation symbols) are across the consecutive months of the extreme event.

GPP losses

To reduce the influence of long-term trends in GPP, we removed the interannual trend [68] and eliminated seasonal variability by subtracting monthly climatological means from the GPP time series. All subsequent analyses were based on the detrended and deseasonalized GPP data. We used the method of Xu et al. (2019) [69] (Fig. S6) to fit a smooth spline curve to the monthly GPP series for each grid cell during the growing season (1982–2018) to represent expected GPP under non-drought conditions. Considering the effects of drought lag [70], we defined the vegetation response time as the period from the onset of drought to the minimum GPP, encompassing both the drought and post-drought lag phases (Fig. S7). GPP losses were calculated over this full response period. Considering the potential lag effects of drought, we set the maximum drought impact period to 12 months, following previous studies [71], and defined the vegetation response time as the interval from the onset of drought to the minimum GPP, covering both the drought and post-drought lag phases (Fig. S7). In addition, we assessed the offset effects between successive droughts [20] by evaluating the likelihood of other drought types occurring during the lag phase and found it to be low (<11%), with minimal influence on the results—i.e., if other types of droughts occurred during the vegetation recovery phase after a drought (such as a low SM), we calculated the proportion of this type of drought to all low SM events. Long term and seasonal trends were removed, so the GPP losses represent pseudo-true values rather than raw observations [6].

Analysis of influencing factors

Vegetation losses caused by drought are influenced by multiple factors. We examined these factors from multiple perspectives, including climatic conditions (precipitation, 2-m temperature, and near-surface solar radiation during droughts), drought characteristics (average duration, frequency, and intensity), and surface factors (soil total nitrogen concentration, soil organic carbon concentration, and elevation).

Human activity also strongly affects the surface, so we selected data for the human footprint in 2018 from Mu et al. (2022) [72] and used human footprint as one of the influencing factors. This data set accurately represented the various pressures humans exerted on the surface environment from 2000 to 2020. It selected eight annual human pressure variables (including built environment, population density, etc.) and assigned values to them separately. These variables were then weighted and aggregated to generate annual human footprint values. The accuracy of the data set was validated through visual interpretation of sample data and showed strong consistency with previously published data sets.

We used geographic detectors to detect spatial heterogeneity and identify its driving forces [73]. This method is used to assess the extent to which factor X explains the spatial variation of attribute Y. We detected the relative importance of each influencing factor on the GPP losses. The computational principles and methods are detailed in Text S1. For a clearer presentation, we used the inverse of the GPP losses calculated in **GPP losses** section. A 7×7-pixel sliding window was then applied to calculate the partial correlations between the GPP losses and the main influencing factors, identified by the results of the analysis of the geographic detectors [74], and pixels with insignificant partial correlation ($p>0.05$) were removed. The specific method for calculating partial correlations is detailed in Text S2.

Recovery time

We defined the period of recovery as the time needed for GPP to increase from the lowest level to the normal level (i.e., when actual GPP was greater than or equal to the fitted GPP at the corresponding time point) [74] (Fig. S7). Vegetation may need many years to recover to normal levels after deforestation, so we removed events where the recovery time exceeded 12 months [75]. When calculating the GPP losses and the time needed to recover from high VPD and low SM, we removed the impact of CDs that occurred at the same time—only high VPD or only low SM was included.

Division of dry and wet areas

The aridity index (AI), defined as the ratio of annual precipitation to annual potential evapotranspiration, was used to identify global wet and dry areas. This metric is routinely used by other researchers [20,76]. Dry

and wet areas were categorized as hyperarid areas (AI<0.05), arid areas (0.05≤AI<0.20), semi-arid areas (0.20≤AI<0.50), dry subhumid areas (0.50≤AI<0.65), subhumid areas (0.65≤AI<1.0) and humid areas (AI ≥1.0) (Fig. S8).

Data availability

Monthly data for precipitation, 2-m temperature, 2-m dew-point temperature, SM, and surface radiation are available from the ERA5 reanalysis dataset (ERA5 monthly averaged data on single levels from 1940 to the present https://cds.climate.copernicus.eu/datasets/reanalysis-era5-single-levels-monthly-means?tab=download). Ground-based observed monthly data for surface 2-m temperature and precipitation are available from the Climatic Research Unit Time Series 4.09 (https://crudata.uea.ac.uk/cru/data/hrg/). GPP data in this study are available from the National Tibetan Plateau Data Center (https://www.tpdc.ac.cn/en/data/d6dff40f-5dbd-4f2d-ac96-55827ab93cc5/). Human-footprint data are available at https://www.x-mol.com/groups/li_xuecao/news/48145. Global data for soil total nitrogen concentration and soil organic carbon concentration (0–100 cm) are from https://www.earthdata.nasa.gov/data/catalog/ornl-cloud-igbp-surfaceproducts-569-1. Vegetation-cover data are available from the ESA/CCI viewer (https://cds.climate.copernicus.eu/datasets/satellite-land-cover?tab=overview).

Funding Statements

C.M. was funded by the National Natural Science Foundation of China (U24A20572, 42521001), and the Fundamental Research Funds for the Central Universities.

Author contribution statements

Yufei Wang: Conceptualization, Data curation, Formal analysis, Investigation, Methodology, Software, Validation, Visualization, Writing – original draft. Chiyuan Miao: Conceptualization, Funding acquisition, Project administration, Writing – review & editing. Chris Huntingford: Investigation, Writing – review & editing. Yuanfang Chai: Investigation, Writing – review & editing. Jiachen Ji: Investigation, Writing – review & editing. Josep Peñuelas: Investigation, Writing – review & editing.

Conflicts of Interest

The authors declare no conflicts of interest.

References

1. Huntingford, C., Burke, E. J., Jones, C. D., Jeffers, E. S. & Wiltshire, A. J. Nitrogen cycle impacts on CO_2 fertilisation and climate forcing of land carbon stores. *Environ. Res. Lett.* **17**, 044072 (2022).
2. Chai, Y. *et al.* Underestimating global land greening: Future vegetation changes and their impacts on terrestrial water loss. *One Earth* **8**, 101176 (2025).
3. Higgins, S. I., Conradi, T. & Muhoko, E. Shifts in vegetation activity of terrestrial ecosystems attributable to climate trends. *Nat. Geosci.* **16**, 147–153 (2023).
4. Linscheid, N. *et al.* Towards a global understanding of vegetation–climate dynamics at multiple timescales. *Biogeosciences* **17**, 945–962 (2020).
5. Piao, S. *et al.* Characteristics, drivers and feedbacks of global greening. *Nat Rev Earth Environ* **1**, 14–27 (2019).
6. Tang, J. *et al.* Shifted trend in drought sensitivity of vegetation productivity from 1982 to 2020. *Agricultural and Forest Meteorology* **362**, 110388 (2025).
7. Li, W. *et al.* Widespread and complex drought effects on vegetation physiology inferred from space. *Nat Commun* **14**, 4640 (2023).
8. Su, J. *et al.* Precipitation observing network gaps limit climate change impact assessment. *Nature* https://doi.org/10.1038/s41586-026-10300-5 (2026) doi:10.1038/s41586-026-10300-5.
9. Chen, L. *et al.* Global increase in the occurrence and impact of multiyear droughts. *Science* **387**, 278–284 (2025).
10. Li, J. *et al.* Future increase in compound soil drought-heat extremes exacerbated by vegetation greening. *Nat*

Commun **15**, 10875 (2024).

11. Yuan, X. *et al.* A global transition to flash droughts under climate change. *Science* **380**, 187–191 (2023).
12. Zhang, Q. *et al.* A new high-resolution multi-drought-index dataset for mainland China. *Earth Syst. Sci. Data* **17**, 837–853 (2025).
13. Seo, K.-W. *et al.* Abrupt sea level rise and Earth's gradual pole shift reveal permanent hydrological regime changes in the 21st century. *Science* **387**, 1408–1413 (2025).
14. Yuan, W. *et al.* Increased atmospheric vapor pressure deficit reduces global vegetation growth. *Sci. Adv.* **5**, eaax1396 (2019).
15. Liu, M. *et al.* Diverging responses of terrestrial ecosystems to water stress after disturbances. *Nat. Clim. Chang.* **15**, 73–79 (2025).
16. Hermann, M., Wernli, H. & Röthlisberger, M. Drastic increase in the magnitude of very rare summer-mean vapor pressure deficit extremes. *Nat Commun* **15**, 7022 (2024).
17. Lu, H. *et al.* Large influence of atmospheric vapor pressure deficit on ecosystem production efficiency. *Nat Commun* **13**, 1653 (2022).
18. Chai, Y. *et al.* Global reduction in sensitivity of vegetation water use efficiency to increasing CO2. *Journal of Hydrology* **641**, 131844 (2024).
19. Hsu, P.-K. *et al.* Raf-like kinases and receptor-like (pseudo)kinase GHR1 are required for stomatal vapor pressure difference response. *Proc. Natl. Acad. Sci. U.S.A.* **118**, e2107280118 (2021).
20. Liu, L. *et al.* Soil moisture dominates dryness stress on ecosystem production globally. *Nat Commun* **11**, 4892 (2020).
21. Zhong, Z. *et al.* Disentangling the effects of vapor pressure deficit on northern terrestrial vegetation productivity. *Sci. Adv.* **9**, eadf3166 (2023).

22. Zhou, S., Zhang, Y., Park Williams, A. & Gentine, P. Projected increases in intensity, frequency, and terrestrial carbon costs of compound drought and aridity events. *Sci. Adv.* **5**, eaau5740 (2019).

23. Sun, W. *et al.* Soil moisture-atmosphere interactions drive terrestrial carbon-water trade-offs. *Commun Earth Environ* **6**, 169 (2025).

24. Fan, X. *et al.* Surging compound drought–heatwaves underrated in global soils. *Proc. Natl. Acad. Sci. U.S.A.* **121**, e2410294121 (2024).

25. He, B., Huang, L., Chen, Z. & Wang, H. Weakening sensitivity of global vegetation to long-term droughts. *Sci. China Earth Sci.* **61**, 60–70 (2018).

26. Wang, S., Zhang, Y., Ju, W., Qiu, B. & Zhang, Z. Tracking the seasonal and inter-annual variations of global gross primary production during last four decades using satellite near-infrared reflectance data. *Science of The Total Environment* **755**, 142569 (2021).

27. Seo, Y.-W. & Ha, K.-J. Changes in land-atmosphere coupling increase compound drought and heatwaves over northern East Asia. *npj Clim Atmos Sci* **5**, 100 (2022).

28. Li, D., An, L., Zhong, S., Shen, L. & Wu, S. Declining coupling between vegetation and drought over the past three decades. *Global Change Biology* **30**, e17141 (2024).

29. Tang, J. *et al.* Seasonal Differences in Vegetation Susceptibility to Soil Drought During 2001–2021. *JGR Biogeosciences* **129**, e2024JG008330 (2024).

30. Wankmüller, F. J. P. *et al.* Global influence of soil texture on ecosystem water limitation. *Nature* **635**, 631–638 (2024).

31. Yang, H. *et al.* The detection and attribution of extreme reductions in vegetation growth across the global land surface. *Global Change Biology* **29**, 2351–2362 (2023).

32. Li, W. *et al.* Widespread increasing vegetation sensitivity to soil moisture. *Nat Commun* **13**, 3959 (2022).

33. Song, J. *et al.* Serious underestimation of reduced carbon uptake due to vegetation compound droughts. *npj Clim Atmos Sci* **7**, 23 (2024).

34. Wu, R., Wang, Z., Meng, F., Liu, Y. & Shi, H. Strengthening Coupling Between Vegetation and Soil-Atmosphere Compound Drought Over the Past Two Decades. *Earth's Future* **13**, e2025EF006311 (2025).

35. Qi, G. *et al.* Increasing impacts of compound extreme droughts on vegetation productivity in China. *Journal of Hydrology* **660**, 133447 (2025).

36. Zhang, W. *et al.* Drought changes the dominant water stress on the grassland and forest production in the northern hemisphere. *Agricultural and Forest Meteorology* **345**, 109831 (2024).

37. Baker, J. C. A. *et al.* An Assessment of Land–Atmosphere Interactions over South America Using Satellites, Reanalysis, and Two Global Climate Models. *Journal of Hydrometeorology* **22**, 905–922 (2021).

38. Novick, K. A. *et al.* The increasing importance of atmospheric demand for ecosystem water and carbon fluxes. *Nature Clim Change* **6**, 1023–1027 (2016).

39. Chen, S., Zhang, Z., Chen, Z., Xu, H. & Li, J. Responses of canopy transpiration and conductance to different drought levels in Mongolian pine plantations in a semiarid urban environment of China. *Agricultural and Forest Meteorology* **347**, 109897 (2024).

40. Green, J. K., Berry, J., Ciais, P., Zhang, Y. & Gentine, P. Amazon rainforest photosynthesis increases in response to atmospheric dryness. *Sci. Adv.* **6**, eabb7232 (2020).

41. Jiao, W. *et al.* Observed increasing water constraint on vegetation growth over the last three decades. *Nat Commun* **12**, 3777 (2021).

42. Zhang, H. *et al.* Increase in plant reliance on past precipitation associated with greening and drying. *Nat Ecol Evol*

https://doi.org/10.1038/s41559-026-02997-4 (2026) doi:10.1038/s41559-026-02997-4.

43. Gharun, M., Shekhar, A., Xiao, J., Li, X. & Buchmann, N. Effect of the 2022 summer drought across forest types in Europe. *Biogeosciences* **21**, 5481–5494 (2024).

44. Song, Y., Jiao, W., Wang, J. & Wang, L. Increased Global Vegetation Productivity Despite Rising Atmospheric Dryness Over the Last Two Decades. *Earth's Future* **10**, e2021EF002634 (2022).

45. Bauke, S. L. *et al.* Soil water status shapes nutrient cycling in agroecosystems from micrometer to landscape scales. *J. Plant Nutr. Soil Sci.* **185**, 773–792 (2022).

46. Yao, Y. *et al.* Compound hot-dry events greatly prolong the recovery time of dryland ecosystems. *National Science Review* nwae274 (2024) doi:10.1093/nsr/nwae274.

47. Belnap, J., Munson, S. M. & Field, J. P. Aeolian and fluvial processes in dryland regions: the need for integrated studies. *Ecohydrology* **4**, 615–622 (2011).

48. Zhang, S., Yang, Y., Wu, X., Li, X. & Shi, F. Postdrought Recovery Time Across Global Terrestrial Ecosystems. *JGR Biogeosciences* **126**, e2020JG005699 (2021).

49. Li, X. *et al.* Global variations in critical drought thresholds that impact vegetation. *National Science Review* **10**, nwad049 (2023).

50. Guo, W. *et al.* Drought trigger thresholds for different levels of vegetation loss in China and their dynamics. *Agricultural and Forest Meteorology* **331**, 109349 (2023).

51. Wu, H. *et al.* Decreasing dynamic predictability of global agricultural drought with warming climate. *Nat. Clim. Chang.* https://doi.org/10.1038/s41558-025-02289-y (2025) doi:10.1038/s41558-025-02289-y.

52. Chen, Y., Zhang, W. & Zhou, T. Increasing exposure of global croplands productivity to growing season heatwaves under climate warming. *Environ. Res. Lett.* **19**, 104073 (2024).

53. Luo, Y. *et al.* Concurrent climate extremes and biological carryover effects dominate severe seasonal reductions in northern vegetation growth. *One Earth* **9**, 101624 (2026).

54. Shi, S., Yang, P., Vrieling, A. & Tol, C. V. D. Vegetation optimal temperature modulates global vegetation season onset shifts in response to warming climate. *Commun Earth Environ* **6**, 203 (2025).

55. Piao, S. *et al.* Plant phenology and global climate change: Current progresses and challenges. *Global Change Biology* **25**, 1922–1940 (2019).

56. Luo, Y. *et al.* Nutrients and water availability constrain the seasonality of vegetation activity in a Mediterranean ecosystem. *Global Change Biology* **26**, 4379–4400 (2020).

57. Samela, C., Imbrenda, V., Coluzzi, R. & Lanfredi, M. Four decades of vegetation phenology across Europe using PKU GIMMS NDVI: assessing timing, stability and spatial patterns. *International Journal of Applied Earth Observation and Geoinformation* **146**, 105041 (2026).

58. Tian, J. *et al.* Slower changes in vegetation phenology than precipitation seasonality in the dry tropics. *Global Change Biology* **30**, e17134 (2024).

59. Wang, S., Yongguang Zhang, & Weimin Ju. Long-term (1982-2018) global gross primary production dataset based on NIRv. 2733842178 Bytes figshare https://doi.org/10.6084/M9.FIGSHARE.12981977.V2 (2020).

60. Yu, J., Wang, W., Chen, Z., Cao, M. & Qian, H. Disentangling the dominance of atmospheric and soil water stress on vegetation productivity in global drylands. *Journal of Hydrology* **657**, 133043 (2025).

61. Wu, H. *et al.* Significant sensitivity of global vegetation productivity to terrestrial surface wind speed changes. *Nat Commun* **16**, 9315 (2025).

62. Li, J. *et al.* Hydroclimatic extremes contribute to asymmetric trends in ecosystem productivity loss. *Commun Earth Environ* **4**, 197 (2023).

63. Hersbach, H. *et al.* The ERA5 global reanalysis. *Quart J Royal Meteoro Soc* **146**, 1999–2049 (2020).

64. Vicente-Serrano, S. M., Beguería, S. & López-Moreno, J. I. A Multiscalar Drought Index Sensitive to Global Warming: The Standardized Precipitation Evapotranspiration Index. *Journal of Climate* **23**, 1696–1718 (2010).

65. Lin, S. *et al.* Global vegetation production may decrease in this century due to rising atmospheric dryness. *Nat Ecol Evol* https://doi.org/10.1038/s41559-025-02885-3 (2025) doi:10.1038/s41559-025-02885-3.

66. Ji, J. *et al.* Transition in Global Basins From Precipitation-Dominated to Evaporative Demand-Dominated Meteorological Drought: Past Patterns and Future Projections. *Earth's Future* **14**, e2025EF007492 (2026).

67. Deng, S. *et al.* Global Distribution and Projected Variations of Compound Drought-Extreme Precipitation Events. *Earth's Future* **12**, e2024EF004809 (2024).

68. Jump, A. S. *et al.* Structural overshoot of tree growth with climate variability and the global spectrum of drought-induced forest dieback. *Global Change Biology* **23**, 3742–3757 (2017).

69. Xu, C. *et al.* Increasing impacts of extreme droughts on vegetation productivity under climate change. *Nat. Clim. Chang.* **9**, 948–953 (2019).

70. Müller, L. M. & Bahn, M. Drought legacies and ecosystem responses to subsequent drought. *Global Change Biology* **28**, 5086–5103 (2022).

71. Zhang, L. *et al.* Lagged and cumulative effects of drought on global vegetation greenness, coverage, and productivity. *Environmental Impact Assessment Review* **115**, 108019 (2025).

72. Mu, H. *et al.* A global record of annual terrestrial Human Footprint dataset from 2000 to 2018. *Sci Data* **9**, 176 (2022).

73. Wang, J. *et al.* Geographical Detectors-Based Health Risk Assessment and its Application in the Neural Tube Defects Study of the Heshun Region, China. *International Journal of Geographical Information Science* **24**, 107–127 (2010).

74. Huang, M. & Zhai, P. Protracted vegetation recovery after compound drought and hot extreme compared to general drought. *Environ. Res. Lett.* **20**, 024001 (2025).

75. Yao, Y., Liu, Y., Zhou, S., Song, J. & Fu, B. Soil moisture determines the recovery time of ecosystems from drought. *Global Change Biology* **29**, 3562–3574 (2023).

76. Elrys, A. S. *et al.* Aridity creates global thresholds in soil nitrogen retention and availability. *Global Change Biology* **30**, e17003 (2024).

Editorial summary:

Compound droughts combining high atmospheric demand and low soil moisture cause the largest global losses of vegetation productivity and slower recovery than single droughts, based on analyses of remotely sensed productivity during the growing season from 1982–2018.

Peer review information:

Communications Earth and Environment thanks the anonymous reviewers for their contribution to the peer review of this work. Primary Handling Editors: Yiming Wang, Mengjie Wang. A peer review file is available.